

Copyright
by
Ryan Patrick Hannigan
2023

The Dissertation Committee for Ryan Patrick Hannigan certifies that
this is the approved version of the following dissertation:

Stranger Things at the LHC

Committee:

Christina Markert, Supervisor

Peter Onyisi

Richard Hazeltine

Chandrajit Bajaj

Stranger Things at the LHC

by

Ryan Patrick Hannigan, B.S.

Dissertation

Presented to the Faculty of the Graduate School of
The University of Texas at Austin
in Partial Fulfillment
of the Requirements
for the degree of
Doctor of Philosophy

The University of Texas at Austin

May, 2023

To Jaynee, who unquestionably is the reason why this document exists.

Stranger Things at the LHC

Publication No. _____

Ryan Patrick Hannigan, Ph.D.
The University of Texas at Austin, 2023

Supervisor: Christina Markert

Among the most mysterious of the four fundamental forces is the strong nuclear force. Responsible for both the binding together of nucleons within an atom, as well as the

Contents

List of Figures	viii
List of Tables	x
Chapter One: Analysis Details	1
1.1 Dataset and event selection	2
1.2 Charged hadron track selection	3
1.3 Λ reconstruction	5
1.4 Reconstruction efficiency	11
1.5 Corrections to the correlation distributions	14
Bibliography	20

List of Figures

1.1	The p_T (left), φ (middle) and η (right) distributions for the trigger hadrons in the multiplicity range 0-20%.	3
1.2	The p_T (left), φ (middle) and η (right) distributions for the associated hadrons in the multiplicity range 0-20%. The dips observed in the φ distribution are due to the TPC sector boundaries.	4
1.3	A diagram depicting a typical V^0 decay with labels for the most important kinematic variables. The diagram was taken from [2].	5
1.4	$n\sigma$ for protons (left) and pions (right) in the TPC detector as a function of p_T	7
1.5	$n\sigma$ for protons (left) and pions (right) in the TOF detector as a function of p_T	8
1.6	$n\sigma$ in TOF vs $n\sigma$ in TPC for protons (left) and pions (right). No contamination is observed for both of the particle species.	8
1.7	Invariant mass distributions in the 0-20% (top), 20-50% (middle), and 50-80% (bottom) multiplicity bins for the Λ candidates which pass the selection criteria with $1.5 < p_T < 2.5$ GeV/ c (left) and $2.5 < p_T < 4.0$ GeV/ c (right). A Voigtian signal + straight-line background fit to the data is shown in blue, with just the background fit shown in red. For these plots, the Λ s were only reconstructed in events with a trigger hadron.	10
1.8	Efficiency vs. p_T for trigger (left) and associated (right) hadrons. While they may look identical, the associated hadron efficiency is slightly lower due to the stricter selection criteria.	12
1.9	Efficiency vs. p_T (left) and η (right) for Λ reconstruction in each multiplicity bin, along with an integrated 0-100% point in red.	13
1.10	2-D non-acceptance corrected h- Λ angular correlations for the 0-20% (top), 20-50% (middle), and 50-80% (bottom) multiplicity bins for $1.5 < p_T < 2.5$ GeV/ c (left) and $2.5 < p_T < 4.0$ GeV/ c (right).	16
1.11	2-D non-acceptance corrected h-h angular correlations for the 0-20% (top), 20-50% (middle), and 50-80% (bottom) multiplicity bins for $1.5 < p_T < 2.5$ GeV/ c (left) and $2.5 < p_T < 4.0$ GeV/ c (right).	17

1.12	2-D mixed-event h- Λ angular correlations for the 0-20% (top), 20-50% (middle), and 50-80% (bottom) multiplicity bins for $1.5 < p_T < 2.5$ GeV/ c (left) and $2.5 < p_T < 4.0$ GeV/ c (right). The Z_{vtx} bins are merged together for these plots.	18
1.13	2-D mixed-event h-h angular correlations for the 0-20% (top), 20-50% (middle), and 50-80% (bottom) multiplicity bins for $1.5 < p_T < 2.5$ GeV/ c (left) and $2.5 < p_T < 4.0$ GeV/ c (right). The Z_{vtx} bins are merged together for these plots.	19

List of Tables

1.1	Number of events passing our criteria for each multiplicity bin considered. Here Z_{vtx} refers to the position of the PV along the beam (z) axis.	2
1.2	The track quality cuts applied to the trigger hadrons in this analysis. . .	3
1.3	The ALICE standard track quality cuts for primary charged hadrons, used for the selection of the associated hadrons in this analysis.	4
1.4	The track quality cuts applied to both the daughter proton and pion tracks used to reconstruct Λ candidates. These cuts are intentionally less strict than those applied to the trigger and associated hadrons as the daughter tracks are reconstructed from secondary particles.	6
1.5	Topological selection criteria applied to Λ candidates.	9

Chapter One: Analysis Details

This chapter builds upon the analysis overview presented in the previous chapter by providing a much more detailed description of each component of the analysis. These components can be summarized as follows. First, a high-quality data sample of p–Pb collisions is selected, with events further differentiated by their multiplicity. Then, quality tracks are selected for the trigger and associated charged hadrons, and the Λ baryons are reconstructed from lower quality tracks using their characteristic decay topology. These Λ daughter tracks are identified as protons or pions using information from the TPC and TOF detectors. Within a given event, the trigger hadrons are then combined with either the associated charged hadrons or the Λ candidates to form pairs, where a distribution of their relative azimuthal angle ($\Delta\varphi \equiv \varphi_{trig.} - \varphi_{assoc.}$) and pseudorapidity ($\Delta\eta \equiv \eta_{trig.} - \eta_{assoc.}$) is filled for each pair. These h- Λ and h-h angular distributions are then corrected for a laundry list of detector effects using both data- and MonteCaro-driven methods. Further corrections are applied to the h- Λ distributions to account for the combinatorial background associated with the Λ reconstruction and the two-track merging effect, whereby one of the daughter tracks gets merged with the trigger hadron track, causing a h- Λ pair deficit at small angles.

The corrected h- Λ and h-h distributions are then projected onto the $\Delta\varphi$ axis to form 1-dimensional azimuthal correlation distributions. These distributions are used to extract the associated per-trigger yields of Λ baryons and charged hadrons in the near- and away-side of the jet, along with the uncorrelated underlying event (UE). Furthermore, the near- and away-side jet widths are extracted from the h- Λ and h-h $\Delta\varphi$ distributions using a von Mises fitting procedure. These observables are all measured in three event multiplicity percentiles (0-20%, 20-50% and 50-80%) and two associated p_T bins ($1.5 < p_T^{assoc.} < 2.5$ GeV/ c and $2.5 < p_T^{assoc.} < 4.0$ GeV/ c).

The structure of this chapter is the following. Section

The systematic uncertainties associated with this analysis are discussed in the next chapter.

1.1 Dataset and event selection

1.1.1 Dataset

Every event in this analysis was a p-Pb collision at $\sqrt{s_{\text{NN}}} = 5.02$ TeV with data collected by the ALICE detector during the 2016 LHC run. This analysis uses the data from these runs with the “FAST” reconstruction, meaning the data was taken without the ITS’s SDD subdetector due to issues with readout during this period. The total number of events (prior to any selection) is roughly 400 million. For the efficiency studies, the analysis was performed using a standard purpose MC-generated production anchored to the dataset using the DPMJET [1] event generator. This production consists of around 400 million minimum bias events, which is roughly equivalent to data.

1.1.2 Event Selection

Events are selected by requiring the location of the primary collision interaction point (called the “primary vertex” or PV) to be no more than 10 cm from the center of the detector along the beam axis or “z”-direction. Furthermore, every event is required to have at least three reconstructed tracks that contributed to the reconstruction of the PV. This reduces the total number of events considered to approximately 350 million events, and a summary of the effects of these selection criteria can be seen in Table 1.1. The events are further separated into three charged particle multiplicity classes (0-20%, 20-50% and 50-80%) based off event activity in the forward-rapidity V0A detector.

Table 1.1: Number of events passing our criteria for each multiplicity bin considered. Here Z_{vtx} refers to the position of the PV along the beam (z) axis.

Multiplicity	Total evts.	Has 3 tracks	$ Z_{vtx} < 10\text{cm} + 3 \text{ tracks}$	% Pass
0-20%	1.0E08	1.0E08	0.8E08	87%
20-50%	1.6E08	1.6E08	1.3E08	86%
50-80%	1.6E08	1.6E08	1.3E08	86%

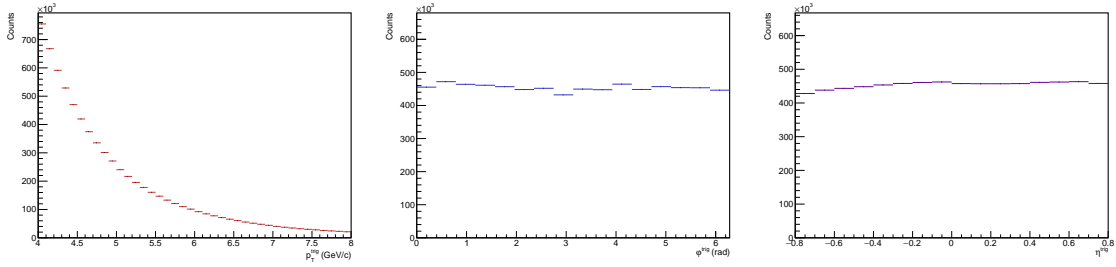


Figure 1.1: The p_T (left), φ (middle) and η (right) distributions for the trigger hadrons in the multiplicity range 0-20%.

1.2 Charged hadron track selection

1.2.1 Trigger track cuts

For any two-particle correlation analysis, the selection criteria of the trigger hadron is of utmost importance as any geometric biases introduced by the trigger selection could be reflected in the final correlation distributions. However, correlation analyses generally require large statistics, thus the selection criteria shown in Table 1.2 are applied to ensure the quality of the trigger hadron track while maximizing the statistics of the analysis. Furthermore, the trigger hadron tracks are required to be at midrapidity ($|\eta| < 0.8$) and have high¹ momentum with $4.0 < p_T^{\text{trig.}} < 8.0$ GeV/c, as the trigger is meant to serve as a proxy for a jet axis. Plots of the p_T , φ and η distributions for the trigger hadrons that pass these cuts in the 0-20% multiplicity bin can be seen in Figure 1.1.

Table 1.2: The track quality cuts applied to the trigger hadrons in this analysis.

Selection criterion	Value
TPC clusters	≥ 50
χ^2 per TPC cluster	< 4
Fraction of shared TPC clusters	< 0.4
DCA_{xy}	< 2.4 cm
DCA_z	< 3.2 cm
Accept kink daughters	No

¹“High” in this case means high enough to guarantee the hadron is produced close (in $\Delta\varphi\Delta\eta$ -space) to a jet axis.

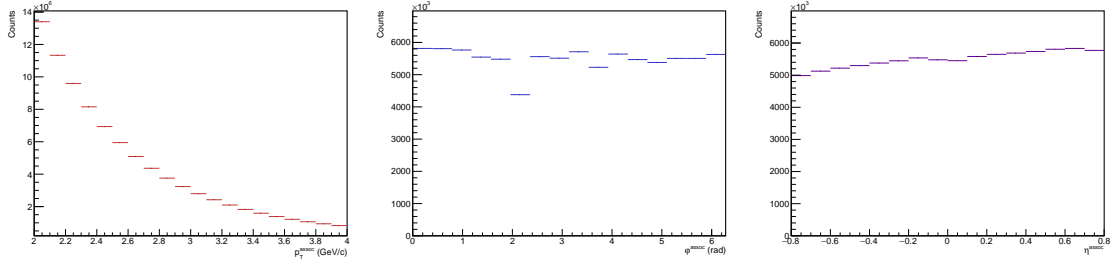


Figure 1.2: The p_T (left), φ (middle) and η (right) distributions for the associated hadrons in the multiplicity range 0-20%. The dips observed in the φ distribution are due to the TPC sector boundaries.

1.2.2 Associated hadron track cuts

To keep the results of this analysis more comparable to previous measurements of the $\Lambda/\pi \approx \Lambda/h$ ratio, the selection criteria for the associated hadrons are more strict than those for the trigger hadrons as the associated hadrons are meant to be “primary”, meaning they did not originate from a weak decay. All associated hadrons are required to meet the ALICE standard track quality cuts for primary charged hadrons described in Table 1.3. Furthermore, the associated hadrons are selected only at midrapidity ($|\eta| < 0.8$) in the momentum region $1.0 < p_T < 4.0 \text{ GeV}/c$, with further binning performed offline. The p_T , φ and η distributions for the associated hadrons that pass these cuts in the 0-20% multiplicity bin can be seen in Figure 1.2.

Table 1.3: The ALICE standard track quality cuts for primary charged hadrons, used for the selection of the associated hadrons in this analysis.

Selection criterion	Value
Crossed rows in TPC	≥ 80
Crossed rows/findable clusters in TPC	> 0.8
TPC clusters	≥ 80
ITS clusters	≥ 3
χ^2 per TPC cluster	< 4
χ^2 per ITS cluster	< 36
TPC and ITS refit required	Yes
DCA_{xy}	$< 0.0105 + 0.0350/p_T^{1.1} \text{ cm}$
DCA_z	$< 2 \text{ cm}$

1.3 Λ reconstruction

1.3.1 Characteristic V^0 decay topology

The Λ candidates in this analysis are reconstructed using their characteristic “V”-shaped decay topology, which is seen in the detector as two oppositely charged tracks originating from a common vertex which is sufficiently displaced from the PV (called the “secondary vertex” or SV). Such particles capable of being reconstructed via this topology are called “ V^0 ”s: the V describing the decay shape and the 0 indicating that the particle is neutral. A diagram depicting a typical V^0 decay is shown in Figure 1.3, with labels given for the most relevant kinematic variables.

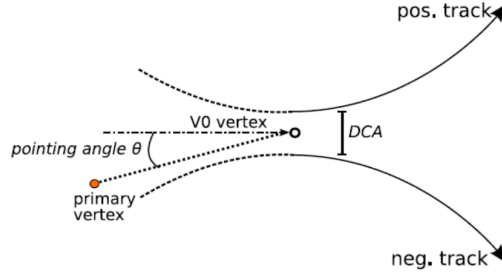


Figure 1.3: A diagram depicting a typical V^0 decay with labels for the most important kinematic variables. The diagram was taken from [2].

The first and most important of these variables is the distance of closest approach (DCA) between the two tracks. This DCA needs to be small enough (relative to the tracking resolution) to ensure that the tracks originated from a common vertex. Another important variable is the transverse decay length of the V^0 , which is the distance between the PV and the SV measured in the xy -plane. The importance of this variable is twofold: if the decay length is too small, then it may not even be possible to resolve the SV from the PV, plus it allows for the distinction between V^0 s of differing decay lengths. The final relevant variable is the cosine of the pointing angle, which is the angle between the momentum vector of the V^0 and the vector pointing from the PV to the SV. As V^0 candidates are generally required to be sufficiently collimated to ensure that the V^0 originated from the PV, the cosine of the pointing angle is usually close to unity.

Using these variables, a list of likely V^0 candidates is generated for each event, from which further cuts are applied to maximize the likelihood of the candidate being a true Λ baryon. These cuts are summarized in the following section. There is also another technique for Λ reconstruction whereby all oppositely charged proton-pion pairs are combined to form Λ candidates, which is explored in more detail in Chapter ???. However, due to the large combinatorial background associated with this technique, the V^0 method described above is nominal for this analysis.

1.3.2 Λ daughter proton and pion track cuts

Because of the longer decay length of the Λ ($c\tau \approx 10$ cm), the corresponding daughter proton and pion tracks generally have fewer hits in both the ITS and TPC, resulting in “lower quality” track parameters. Because of this, the cuts applied to the daughter tracks used to reconstruct Λ candidates are the least strict of all the track quality cuts in this analysis and are summarized in Table 1.4. The daughter proton and pion are also required to be at midrapidity ($|\eta| < 0.8$) and have a minimum p_T of $p_T > 0.15$ GeV/ c .

Table 1.4: The track quality cuts applied to both the daughter proton and pion tracks used to reconstruct Λ candidates. These cuts are intentionally less strict than those applied to the trigger and associated hadrons as the daughter tracks are reconstructed from secondary particles.

Selection criterion	Value
TPC refit required	Yes
Crossed rows in TPC	≥ 70
Crossed rows/findable clusters in TPC	> 0.8

Following the particle identification procedure outlined in Sections ?? and ??, the daughter proton and pion tracks are required to pass the following PID cuts using both the TPC and TOF detectors:

- $|n\sigma_{\text{TPC},p}| < 2$
- $|n\sigma_{\text{TPC},\pi}| < 3$
- $|n\sigma_{\text{TOF},p}| < 2$ (if signal exists)
- $|n\sigma_{\text{TOF},\pi}| < 3$ (if signal exists)

The values of these cuts were chosen to maximize the Λ signal while avoiding contamination from other particle species. The parenthetical “if signal exists” means that the TOF PID cut is only applied if the track has a TOF signal. Due to the large distance between the TOF detector and the PV, many lower momentum tracks are deflected by the magnetic field before reaching the TOF detector, resulting in no signal. Excluding such tracks results in a more pure sample of protons and pions, at the cost of a much lower number of Λ candidates. While such a cost is not acceptable for the nominal analysis, the effect of excluding these tracks is investigated in Chapter ??.

The $n\sigma$ distributions for both the TPC and TOF detectors of the daughter proton and pion tracks that pass the aforementioned quality cuts are shown in Figure 1.4 and Figure 1.5, respectively. To check for contamination from other particle species, the TOF and TPC information is combined to form a $n\sigma_{\text{TOF}}$ vs $n\sigma_{\text{TPC}}$ plot, which is shown for both the protons and pions in Figure 1.6. No contamination is observed for either the proton or pion tracks.

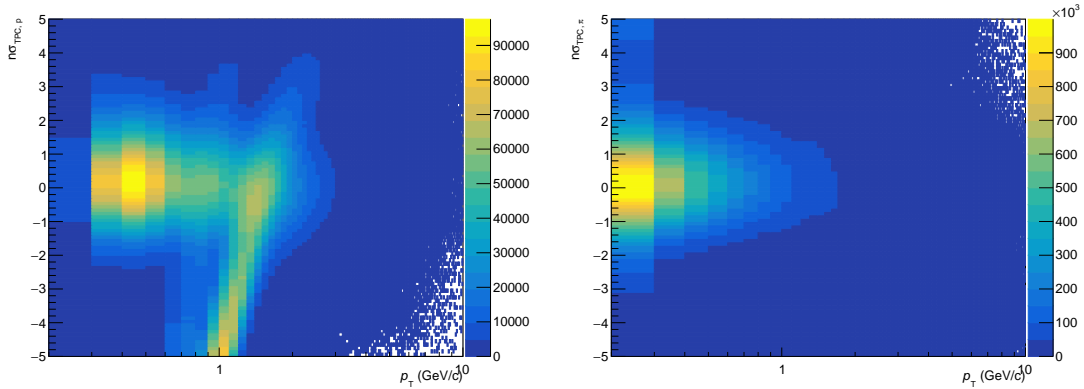


Figure 1.4: $n\sigma$ for protons (left) and pions (right) in the TPC detector as a function of p_T .

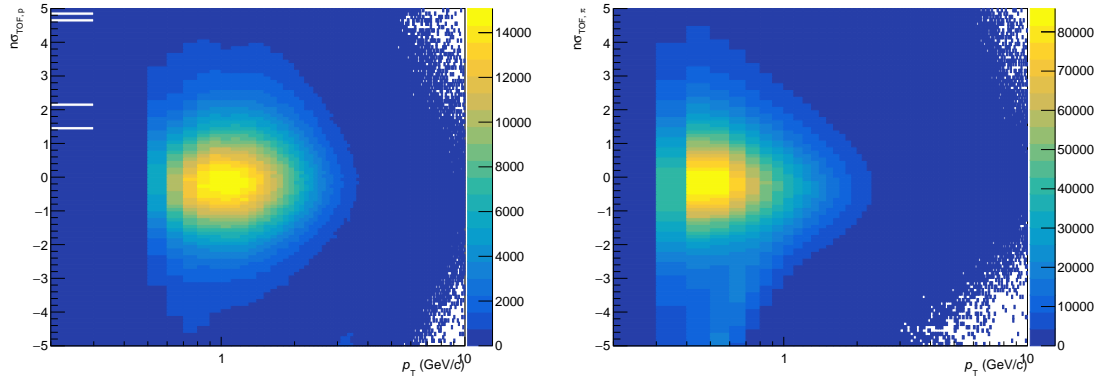


Figure 1.5: $n\sigma$ for protons (left) and pions (right) in the TOF detector as a function of p_T .

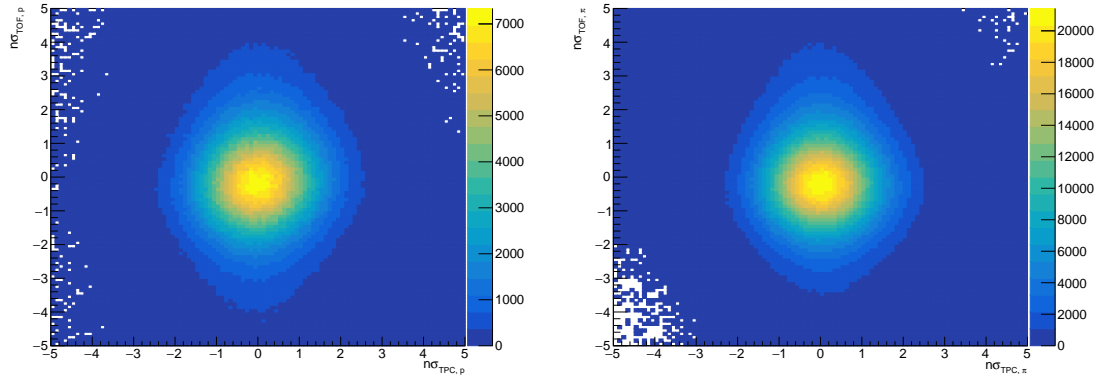


Figure 1.6: $n\sigma$ in TOF vs $n\sigma$ in TPC for protons (left) and pions (right). No contamination is observed for both of the particle species.

1.3.3 Λ candidate selection

With the daughter proton and pion tracks selected, the Λ candidates are generated by combining all oppositely charged proton-pion pairs into V^0 s which meet the topological selection criteria described in Table 1.5.

Table 1.5: Topological selection criteria applied to Λ candidates.

Selection criterion	Value
$ \eta $	< 0.8
Decay radius (cm)	> 0.2
DCA _{xy} of pion track to PV (cm)	> 0.06
DCA _{xy} of proton track to PV (cm)	> 0.06
DCA _{xy} between daughter tracks ($n\sigma$)	< 1.5
$\cos(\theta_{\text{pointing}})$	> 0.9
Invariant mass (GeV/c^2)	$1.102 < M_{p\pi} < 1.130$

The invariant mass $M_{p\pi}$ is calculated using

$$M_{p\pi} = \sqrt{(E_p + E_\pi)^2 - (\vec{p}_p + \vec{p}_\pi)^2}, \quad (1.1)$$

where $E_x = \sqrt{m_x^2 + p_x^2}$ is the energy of the particle of species x . The $M_{p\pi}$ distributions for the Λ candidates for all multiplicity and momentum bins are shown in Figure 1.7. The distributions are also fit with a Voigtian function (convolution of Breit-Wigner and Gaussian [3]) plus a straight line to describe the background. Note that despite our selection criteria, there is still a non-negligible background due to the presence of misidentified Λ candidates. As this background inevitably makes its way into the final h- Λ correlation distributions, it is removed using the technique described in Section ??.

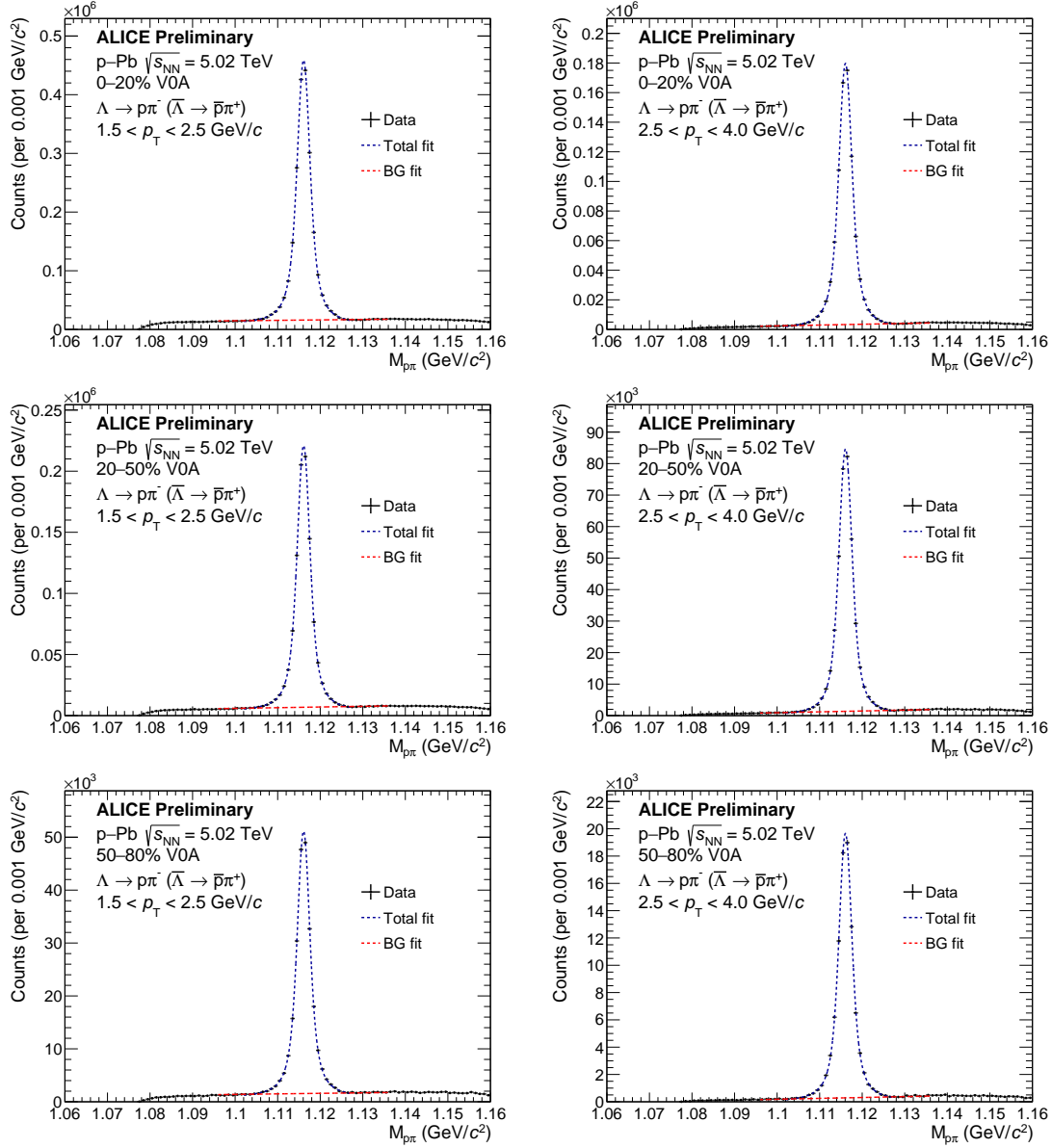


Figure 1.7: Invariant mass distributions in the 0-20% (top), 20-50% (middle), and 50-80% (bottom) multiplicity bins for the Λ candidates which pass the selection criteria with $1.5 < p_T < 2.5$ GeV/c (left) and $2.5 < p_T < 4.0$ GeV/c (right). A Voigtian signal + straight-line background fit to the data is shown in blue, with just the background fit shown in red. For these plots, the Λ s were only reconstructed in events with a trigger hadron.

1.4 Reconstruction efficiency

In an ideal world, the number of reconstructed particles of interest would be equal to the number of particles produced in the collision. Unfortunately this is not the case, as there are a number of detector effects which can cause particles to be “lost” during reconstruction. To correct for these effects, the reconstruction efficiency

$$\epsilon(x_1, x_2, \dots, x_n) \equiv P(f(x_1, x_2, \dots, x_n)|g(x_1, x_2, \dots, x_n)), \quad (1.2)$$

is used. Here x_i are the kinematic variables of the particle of interest (e.g. p_T , η , φ), $f(x_1, x_2, \dots, x_n)$ is the probability that a particle is reconstructed (“found”) with kinematic variables x_i , and $g(x_1, x_2, \dots, x_n)$ is the probability that a particle is produced (“generated”) with the same variables. While the distributions f and g are inaccessible within a given event, the efficiency can be calculated using Monte Carlo simulation techniques via the equation

$$\epsilon(x_1, x_2, \dots, x_n) = \frac{N_{\text{reco.}}(x_1, x_2, \dots, x_n)}{N_{\text{gen.}}(x_1, x_2, \dots, x_n)}, \quad (1.3)$$

where $N_{\text{reco.}}$ and $N_{\text{gen.}}$ are the reconstructed and generated particle distributions, respectively, usually taken across a large number of simulated events. In this analysis, these distributions are calculated as a function of p_T and η for each multiplicity class using 30 million events generated by the Monte Carlo event generator DPMJET [1] with particle propagation through the ALICE detector performed by the GEANT3 [4] detector simulation software. These efficiency distributions are then used to correct the h- Λ and h-h correlation distributions using the procedure described in Section 1.5.

1.4.1 Charged hadron reconstruction efficiency

The trigger and associated hadron track reconstruction efficiencies are calculated using Equation 1.3, where the trigger and associated hadrons from $N_{\text{reco.}}$ are subject to the following:

- The track passes the quality cuts outlined in Tables 1.2 (trigger) or 1.3 (associated)
- The track has a corresponding generated particle
- That generated particle is either a pion, proton, kaon, electron or muon

- $|\eta_{\text{track}}| \leq 0.8$,

and the trigger and associated hadrons from $N_{\text{gen.}}$ are subject to:

- $|\eta_{\text{track}}| \leq 0.8$
- The particle is either a pion, proton, kaon, electron or muon
- The particle is primary (i.e. did not originate from a weak decay)

The trigger and associated track reconstruction efficiencies are shown for each multiplicity class as a function of p_T in Figure 1.8. While these efficiencies exhibit relatively flat behavior as a function of p_T and multiplicity, they are still treated as p_T and multiplicity dependent during the correction procedure.

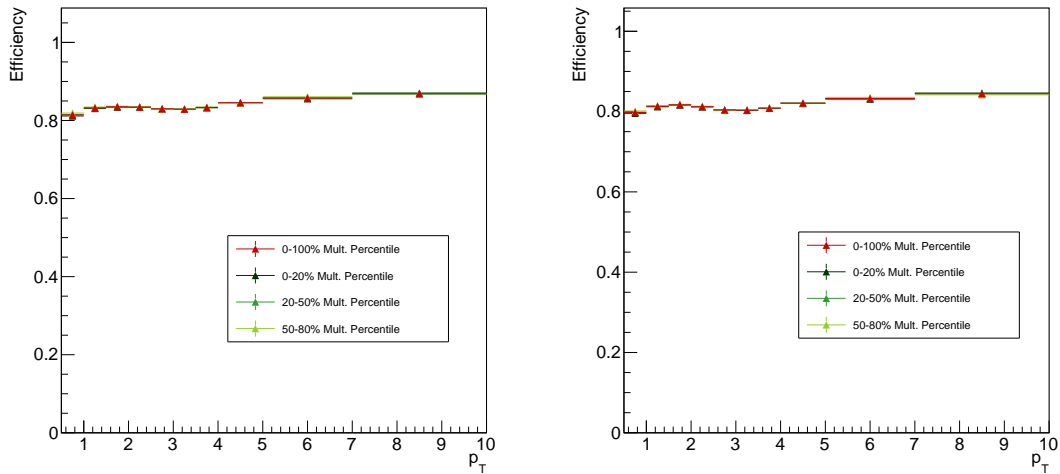


Figure 1.8: Efficiency vs. p_T for trigger (left) and associated (right) hadrons. While they may look identical, the associated hadron efficiency is slightly lower due to the stricter selection criteria.

1.4.2 Λ reconstruction efficiency

The Λ reconstruction efficiency is calculated as a function of p_T and η using Equation 1.3, where the Λ s from $N_{\text{reco.}}$ are subject to the following:

- They pass the topological selection criteria from Table 1.5

- The reconstructed daughter p, π tracks pass the quality cuts from Table 1.4
- The daughter p, π tracks have corresponding generated p, π particles
- Those generated p, π daughters come from the same mother Λ
- $|\eta_\Lambda| \leq 0.8$,

and the Λ s from $N_{\text{gen.}}$ are subject to:

- $|\eta_\Lambda| \leq 0.8$
- The Λ decays to $p\pi$.

The requirement that the generated Λ s decay into $p\pi$ means the branching ratio is not included in the efficiency calculation as it is corrected for separately (see Section 1.5). The Λ reconstruction efficiency can be seen for each multiplicity class as a function of p_T and η in Figure 1.9. Note that the efficiency is no longer flat as a function of η due to the $|\eta| < 0.8$ requirement for the daughter tracks, which kinematically restricts the Λ reconstruction to a smaller η range.

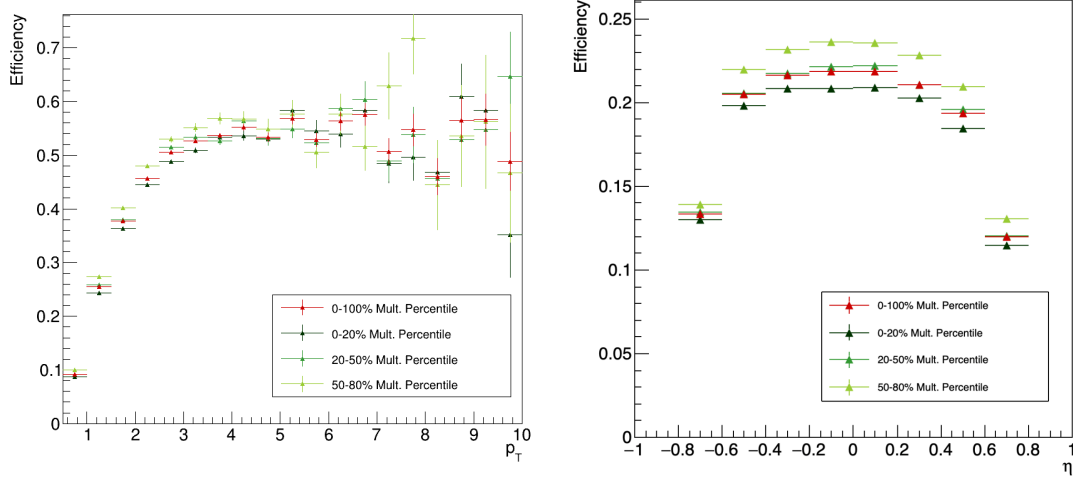


Figure 1.9: Efficiency vs. p_T (left) and η (right) for Λ reconstruction in each multiplicity bin, along with an integrated 0-100% point in red.

1.5 Corrections to the correlation distributions

Once the trigger and associated particles are selected, the two-particle h- Λ and h-h correlation distributions are generated. As mentioned in the previous chapter, the corrected two-particle correlation function is given by

$$\frac{1}{N_{trig}} \frac{d^2 N_{pair}}{d\Delta\varphi d\Delta\eta} = \frac{1}{N_{trig}^{corr}} \frac{1}{\epsilon_{trig} \times \epsilon_{assoc}} B(0,0) \frac{S(\Delta\varphi, \Delta\eta)}{B(\Delta\varphi, \Delta\eta)} \frac{1}{\epsilon_{pair}(\Delta\varphi, \Delta\eta)}. \quad (1.4)$$

which contains a number of explicit correction terms (in the form of ϵ s) along with some implicit corrections. These corrections are described in this section, and are presented in the order in which they are applied to the data.

1.5.1 Single-particle efficiency corrections

As both the trigger and the associated particles have their own independent reconstruction efficiencies, the trigger-associated pair reconstruction efficiency should be

$$\epsilon_{trig,assoc} = \epsilon_{trig} \times \epsilon_{assoc}, \quad (1.5)$$

meaning the single-particle efficiency distributions from Section 1.4 can be used to calculate the weight $1/(\epsilon_{trig} \times \epsilon_{assoc})$. This weight is applied for each h- Λ and h-h pair in the two-dimensional correlation distribution. However, the assumption that the reconstruction efficiencies are independent is slightly incorrect in the case of the h- Λ distributions due to track merging effects, thus an additional ϵ_{pair} correction is required (discussed in detail in Section ??).

The trigger efficiency weight $1/\epsilon_{trig}$ is also applied to the single-particle trigger hadron distribution in data to obtain N_{trig}^{corr} .

1.5.2 Mixed-event acceptance correction

As mentioned in Section ??, the $B(0,0)/B(\Delta\varphi, \Delta\eta)$ term in Equation 1.4 corrects for the finite acceptance along η as both our trigger and associated particles are required to be within $|\eta| < 0.8$. The mixed-event distribution $B(\Delta\varphi, \Delta\eta)$ shown in Figure ?? has a characteristic triangular shape along $\Delta\eta$, which is purely due to detector geometry as no physical correlations are present. When scaled by $1/B(0,0)$, the mixed event distribution becomes the probability that a particle pair is found given

that the trigger particle is within $|\eta| < 0.8$, which is unity at $\Delta\varphi, \Delta\eta = 0, 0$. Thus correcting the same-event distribution $S(\Delta\varphi, \Delta\eta)$ by $B(0, 0)/B(\Delta\varphi, \Delta\eta)$ removes this acceptance effect and allows for a more accurate determination of the pair-wise yields.

While the generation of the mixed event distribution $B(\Delta\varphi, \Delta\eta)$ was discussed briefly in Section ??, the specific details are as follows. First, in order to ensure that the mixed-event pairs are coming from similar events, the events in the mixing pool are separated by both multiplicity percentile and Z_{vtx} position. The categorizing of events based off of Z_{vtx} position is an integral part of the acceptance correction: events with a Z_{vtx} at one edge of the detector have a completely different (and nearly inverted) η acceptance than those on the opposite edge. The multiplicity bins are the same as they are for the same-event distributions (namely 0-20%, 20-50% and 50-80%), and the ten Z_{vtx} bins are split evenly from -10 cm to 10 cm. For each multiplicity and Z_{vtx} bin, the acceptance correction

$$S_{\text{corr.}}(\Delta\varphi, \Delta\eta) = \frac{S(\Delta\varphi, \Delta\eta)}{B(\Delta\varphi, \Delta\eta)/B(0, 0)} \quad (1.6)$$

is performed, and the results for each multiplicity bin are then merged across all Z_{vtx} bins. The uncorrected distributions $S(\Delta\varphi, \Delta\eta)$ and the mixed-event distributions $B(\Delta\varphi, \Delta\eta)$ are shown for both the h- Λ and h-h cases for all multiplicity and associated momentum bins in Figures 1.10 through 1.13.

This mixed-event correction is the final correction applied to the h-h distributions. However, the h- Λ distributions require additional corrections that are not present in the dihadron case.

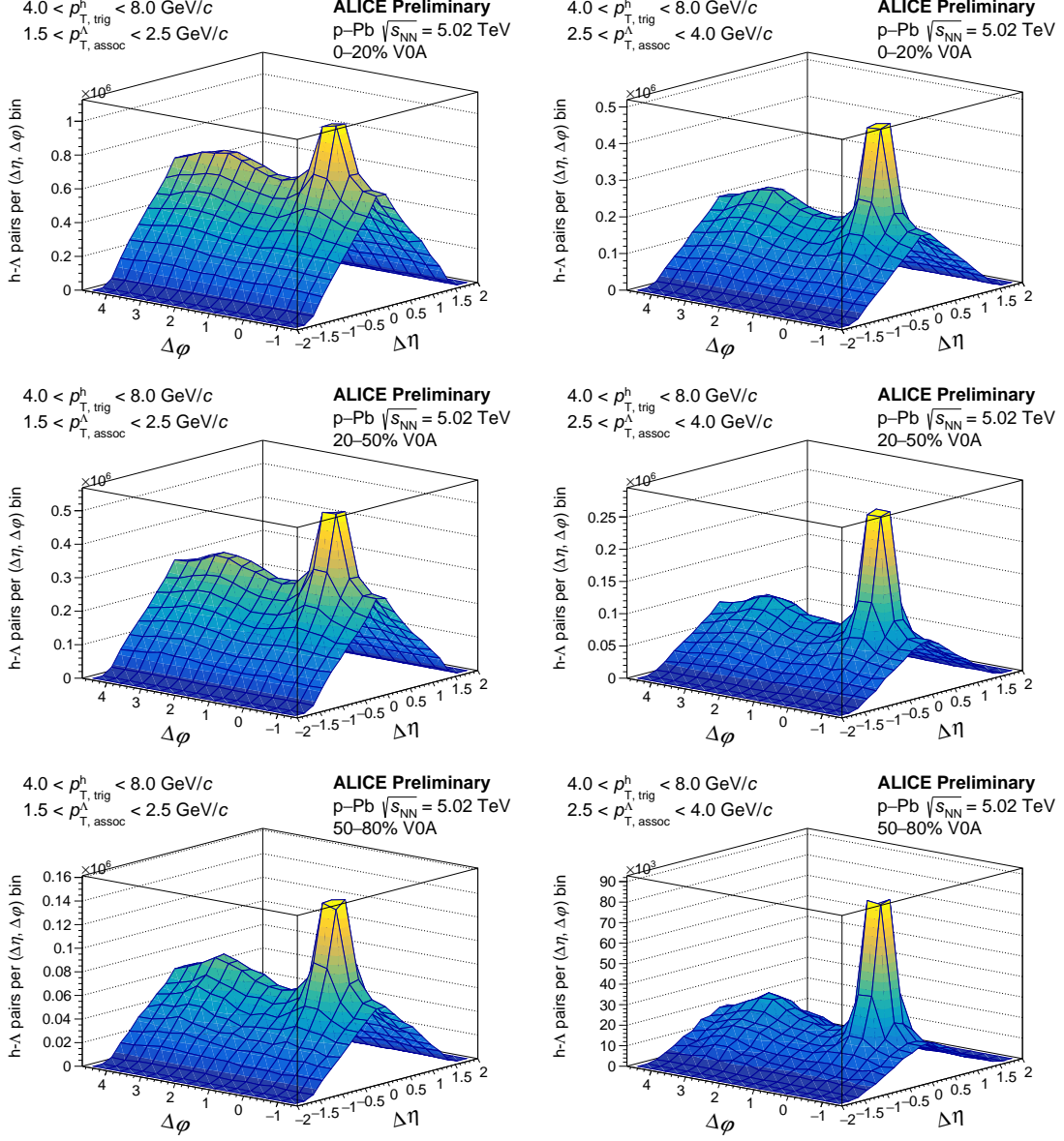


Figure 1.10: 2-D non-acceptance corrected h - Λ angular correlations for the 0-20% (top), 20-50% (middle), and 50-80% (bottom) multiplicity bins for $1.5 < p_T < 2.5$ GeV/c (left) and $2.5 < p_T < 4.0$ GeV/c (right).

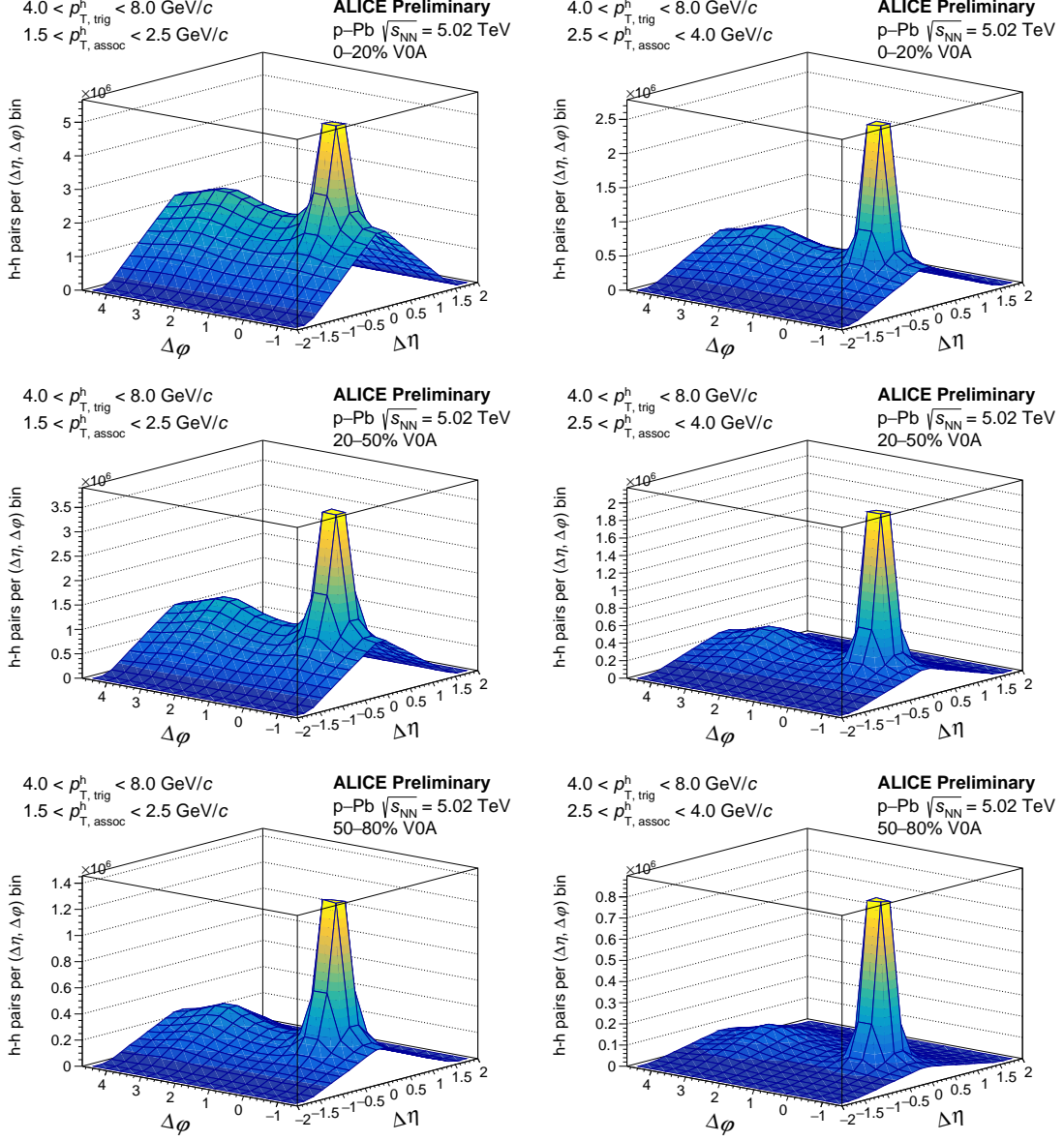


Figure 1.11: 2-D non-acceptance corrected h-h angular correlations for the 0-20% (top), 20-50% (middle), and 50-80% (bottom) multiplicity bins for $1.5 < p_T < 2.5$ GeV/c (left) and $2.5 < p_T < 4.0$ GeV/c (right).

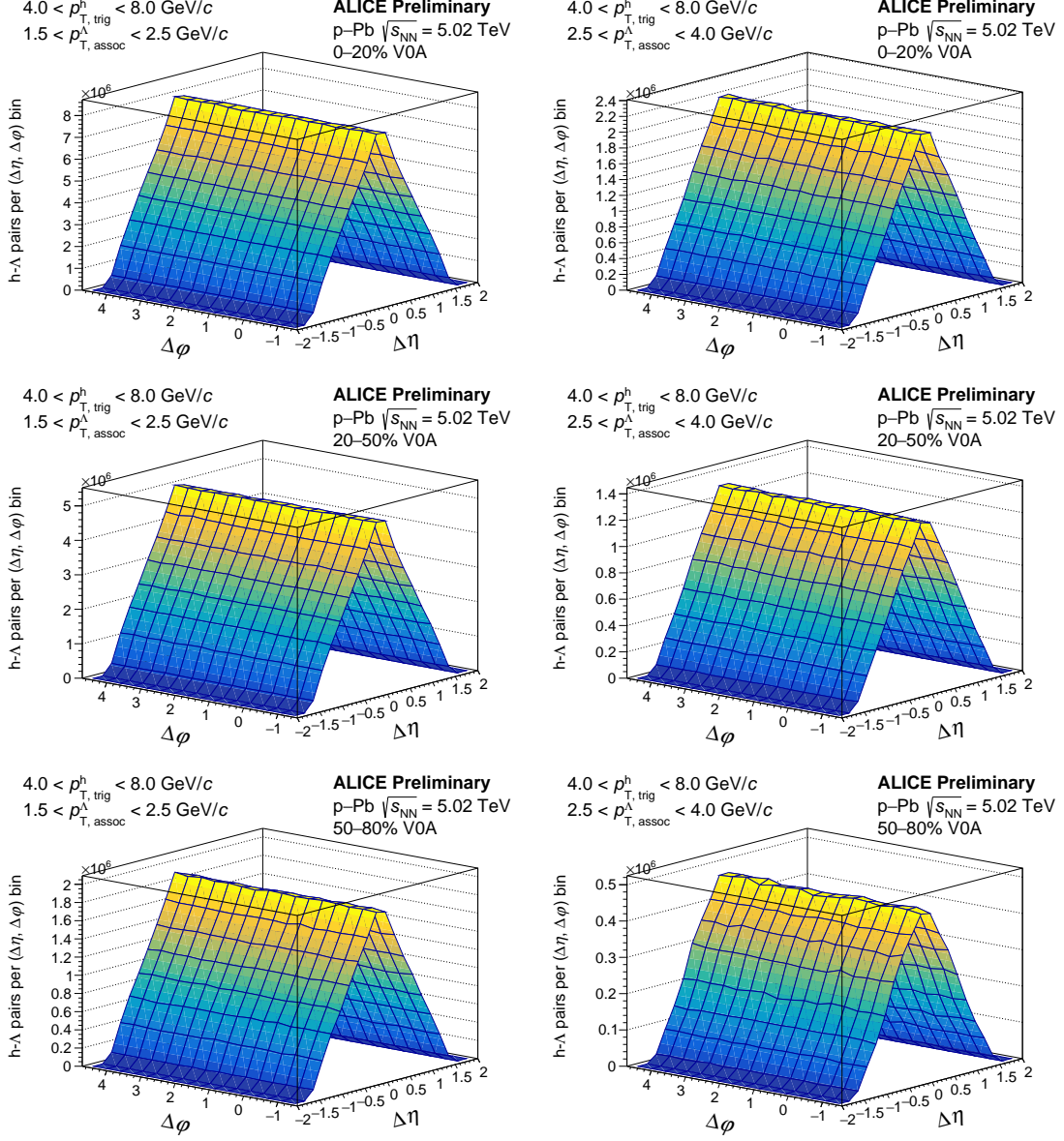


Figure 1.12: 2-D mixed-event h - Λ angular correlations for the 0-20% (top), 20-50% (middle), and 50-80% (bottom) multiplicity bins for $1.5 < p_T < 2.5 \text{ GeV}/c$ (left) and $2.5 < p_T < 4.0 \text{ GeV}/c$ (right). The Z_{vtx} bins are merged together for these plots.

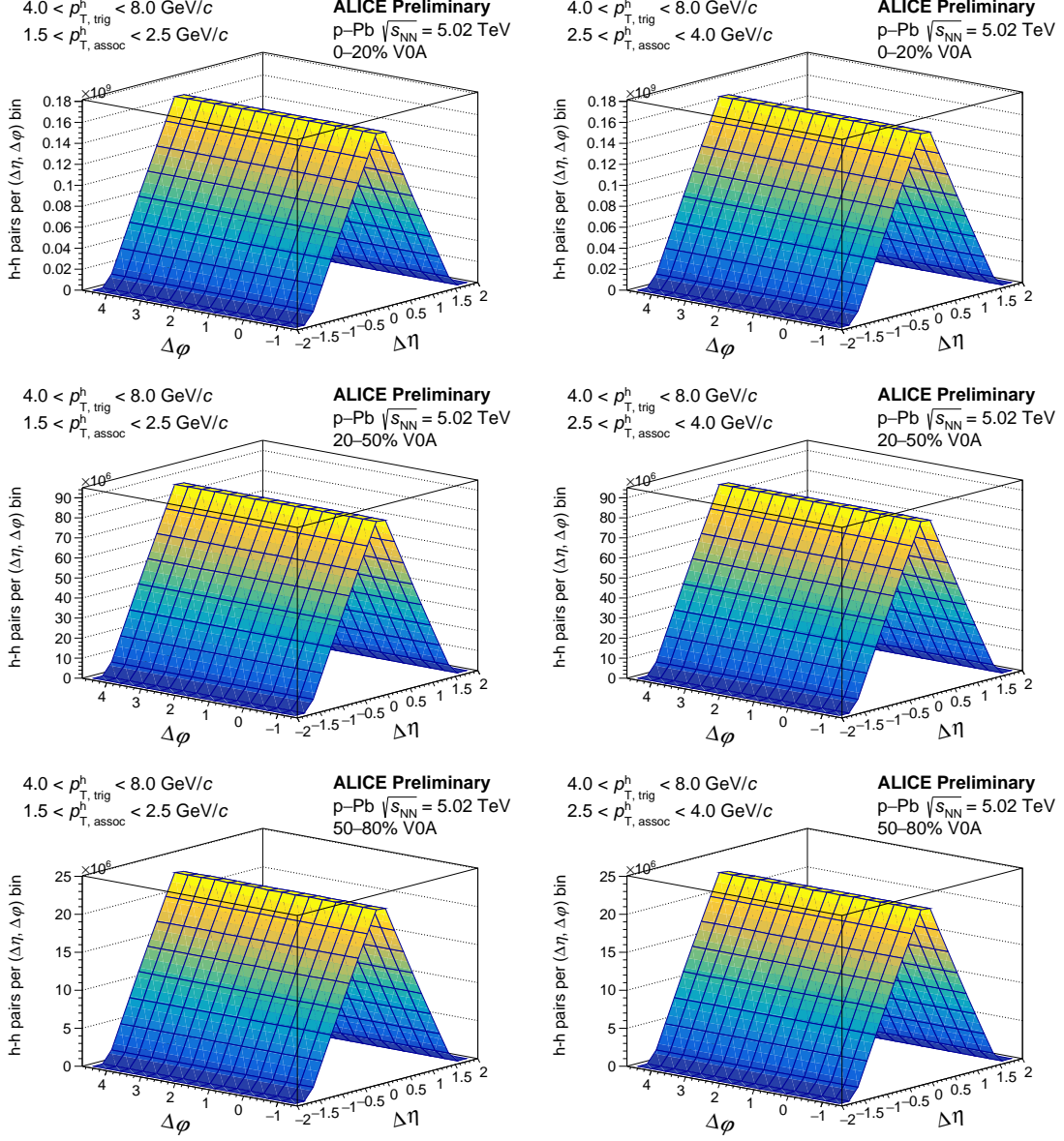


Figure 1.13: 2-D mixed-event h-h angular correlations for the 0-20% (top), 20-50% (middle), and 50-80% (bottom) multiplicity bins for $1.5 < p_T < 2.5 \text{ GeV}/c$ (left) and $2.5 < p_T < 4.0 \text{ GeV}/c$ (right). The Z_{vtx} bins are merged together for these plots.

Bibliography

- [1] S. Roesler, R. Engel, and J. Ranft, “The monte carlo event generator DPMJET-III,” in *Advanced Monte Carlo for Radiation Physics, Particle Transport Simulation and Applications*, Springer Berlin Heidelberg, 2001. arXiv: 0012252 [hep-ph] (cit. on pp. 2, 11).
- [2] A. Kalweit, *Energy loss calibration of the ALICE TPC*, 2008 (cit. on p. 5).
- [3] S. Acharya *et al.*, “Production of $K^*(892)^0$ and $\phi(1020)$ in pp and p-Pb collisions at $\sqrt{s_{NN}} = 5.02$ tev,” *Phys. Rev.*, vol. C97, 2022. DOI: 10.1103/physrevc.106.034907. [Online]. Available: <https://doi.org/10.1103/physrevc.106.034907> (cit. on p. 9).
- [4] R. Brun *et al.*, *GEANT: Detector Description and Simulation Tool; Oct 1994*, ser. CERN Program Library. Geneva: CERN, 1993, Long Writeup W5013. DOI: 10.17181/CERN.MUHF.DMJ1. [Online]. Available: <http://cds.cern.ch/record/1082634> (cit. on p. 11).